Kirigami-enabled self-folding origami

van Manen, Teunis; Janbaz, Shahram; Ganjian, Mahya; Zadpoor, Amir A.

Important note
To cite this publication, please use the final published version (if applicable).
Please check the document version above.

Kirigami-enabled self-folding origami

Teunis van Manen *, Shahram Janbaz, Mahya Ganjian, Amir A. Zadpoor

Additive Manufacturing Laboratory, Department of Biomechanical Engineering, Delft University of Technology (TU Delft), Mekelweg 2, Delft 2628CD, The Netherlands

Self-folding of complex origami-inspired structures from flat states allows for the incorporation of a multitude of surface-related functionalities into the final 3D device. Several self-folding techniques have therefore been developed during the last few years to fabricate such multi-functional devices. The vast majority of such approaches are, however, limited to simple folding sequences, specific materials, or large length scales, rendering them inapplicable to microscale (meta)materials and devices with complex geometries, which are often made from materials other than the ones for which these approaches are developed. Here, we propose a mechanical self-folding technique that only requires global stretching for activation, is applicable to a wide range of materials, allows for sequential self-folding of multi-storey constructs, and can be downscaled to microscale dimensions. We combined two types of permanently deforming kirigami elements, working on the basis of either multi-stability or plastic deformation, with an elastic layer to create self-folding basic elements. The folding angles of these elements could be controlled using the kirigami cut patterns as well as the dimensions of the elastic layer and be accurately predicted using our computational models. We then assembled these basic elements in a modular manner to create multiple complex 3D structures (*e.g.*, multi-storey origami lattices) in different sizes including some with microscale feature sizes. Moreover, starting from a flat state enabled us to incorporate not only precisely controlled, arbitrarily complex, and spatially varied micropatterns but also flexible electronics into the self-folded 3D structures. In all cases, our computational models could capture the self-folding behavior of the assemblies and the strains in the connectors of the flexible electronic devices, thereby guiding the rational design of our specimens. This approach has numerous potential applications including fabrication of multi-functional and instrumented implantable medical devices, steerable medical instruments, and microrobots.

Introduction

Self-folding origami [1–3] has a myriad of potential applications in the development of designer materials with advanced functionalities including robotic materials [4–7], thin film materials [8], mechanical metamaterials [9–13], optical metamaterials [14], electronic devices [15], antennas [16], space structures [17–18], and biomaterials [19–21]. Self-folding origami can, therefore, be seen as an alternative fabrication strategy with advantages that range from lower manufacturing costs to enabling the combination of the favorable properties offered by 2D materials with those of bespoke 3D structures. In particular, shape-shifting materials that allow for the formation of complex 3D geometries from initially flat materials offer a promising

* Corresponding author.
    E-mail address: van Manen, T. (t.vanmanen@tudelft.nl)

1

strategy for the fabrication of surface-functionalized lattice structures [20]. Given the fact that the geometrical design of many metamaterials with various types of rare or unprecedented properties are based on regular lattice structures [22–27], self-folding origami lattices hold particular promise in this regard. For this type of advanced metamaterials, starting from a flat state would also allow for the use of advanced production techniques that are usually only applicable to flat surfaces, such as electron beam nanolithography [28–30], dip pen nanolithography [31,32], and direct-write atomic layer deposition [33]. These techniques could then be used to embed a variety of complex surface features in the flat material prior to the assembly into a 3D structure. That may include printable electronic devices that incorporate sensors and actuators into the ultimate (wearable) 3D object [15,16,34,35], surface nanopatterns that determine stem cell fate [36–38] or kill bacteria to prevent implant-associated infections [39,40], or surface nano-features that manipulate the surface properties to create superhydrophobicity or superhydrophilicity [41–43] for such applications as self-cleaning surfaces. In this approach, once the incorporation of the surface-related functionalities is concluded, a self-folding behavior is initiated using a triggering stimulus.

Different strategies based on either internally generated stresses or externally applied forces have been proposed for the fabrication of stimuli-responsive materials that shift their shape from a flat state to a 3D geometry [1,3,44]. Internal stresses could be generated using shape-memory polymers or alloys that exhibit dimensional changes upon activation by a variety of stimuli including temperature [45–47] and humidity [48]. Based on the arrangement of those active materials, out-of-plane deformations can be programmed into a flat material [1,3]. However, the application of these approaches is limited by the type of activation stimulus. For example, active materials that require high temperatures for activation cannot be used inside the human body. Moreover, this strategy requires the use of specific materials, which is an important limiting factor for many applications. Finally, this approach is not suited for the fabrication of self-folding origami (lattices) at smaller scales, as accurate positioning and/or training of (shape-memory) materials at the microscale may be needed. In the case of 4D printing approaches [49,50], the dimensional accuracy required for microscale fabrication of self-folding origami often exceeds the resolution of the available 3D printing technologies.

The alternative approach of working with external forces could help overcome most of the above-mentioned challenges. However, design flexibility is much reduced when working with a few globally applied forces. It is therefore extremely challenging to program complex shape-shifting behaviors such as those required for the folding of regular lattices from flat states. A variety of shape-shifting techniques based on externally applied forces have been reported in the literature [51]. For example, capillary forces have been utilized for the folding of polyhedral structures [52]. Nevertheless, only simple 3D geometries comprising a single polyhedral unit cell have, thus far, been demonstrated [53]. Compressive buckling of thin stiff constructs on top of a pre-stressed elastomeric substrate has also been used for the fabrication of 3D geometries from initial flat state [54]. However, the actuation forces have to be applied locally through a pre-

cisely controlled pattern of bonding sites between the construct and substrate, which limits the fabrication of complex freestanding and multi-storey constructs.

Here, we propose a new kirigami-based approach for the design and fabrication of self-folding origami-like structures, ranging from simple cubes [53,55,56] to complex polyhedral lattices [20], that are activated with externally-applied (i.e., global) mechanical forces. The presented approach is suitable for the fabrication of self-folding origami at the microscale and is applicable to a wide range of materials. Furthermore, we work with tensile forces as opposed to the buckling-inducing compressive forces that had been used in some previous studies [54]. The use of tensile forces enables us to inhibit global buckling patterns whose behavior may be challenging to predict in the nonlinear post-buckling regime. Taking advantage of the multi-stability [57–59] and highly localized out-of-plane buckling [60–64], our approach also lends itself to sequential self-folding that is crucial for multi-step folding strategies.

Results and discussion
Self-folding elements
We used a combination of experimental techniques and computational models to design, fabricate, and analyze our self-folding origami-inspired structures (see Materials and Methods). The main concept in this approach is a through-the-thickness combination of an elastic layer with a layer exhibiting permanent deformation. The permanent deformation may arise from multi-stability or from the plastic deformation of the material. The presented shape-shifting concepts could, therefore, be applied to different types of materials (e.g., metals and polymers). When stretched, both layers will elongate. Upon the release of the force, the elastic layer tends to contract back to its original length, while the permanently-deformed layer opposes that recovery. The mismatch between the tendencies of both layers causes an out-of-plane deformation that could be exploited to self-fold initially flat constructs.

We implemented this approach by designing two types of kirigami elements that exhibited permanent deformations upon stretching (Fig. 1a). We then combined the kirigami elements with a layer of an elastomeric material (i.e., PDMS) to create self-folding bilayers (Fig. 1a). Shape transformations could be programmed using different arrangements of these basic elements. We fabricated our kirigami elements from both multi-stable polymer sheets (Fig. 1b) as well as from metal foils (Fig. 1b). A pattern of mutually orthogonal cuts into a polyolefin sheet caused the material to exhibit a multi-stable mechanical response. Upon stretching above a critical strain value, the four square elements present within the kirigami element rotated far enough to 'snap' into their other stable position, thereby elongating the kirigami strip permanently (Fig. 1c). The elastic energy stored in the arms of the bistable elements during the process of stretching will be released once the critical (snapping) point has been passed, resulting in a negative stiffness. The amount of the permanent elongation could be adjusted by changing the dimensions of the elements constituting the kirigami strip such as the dimensions of the square elements (Fig. 1c). Other parameters such as the dimensions of the
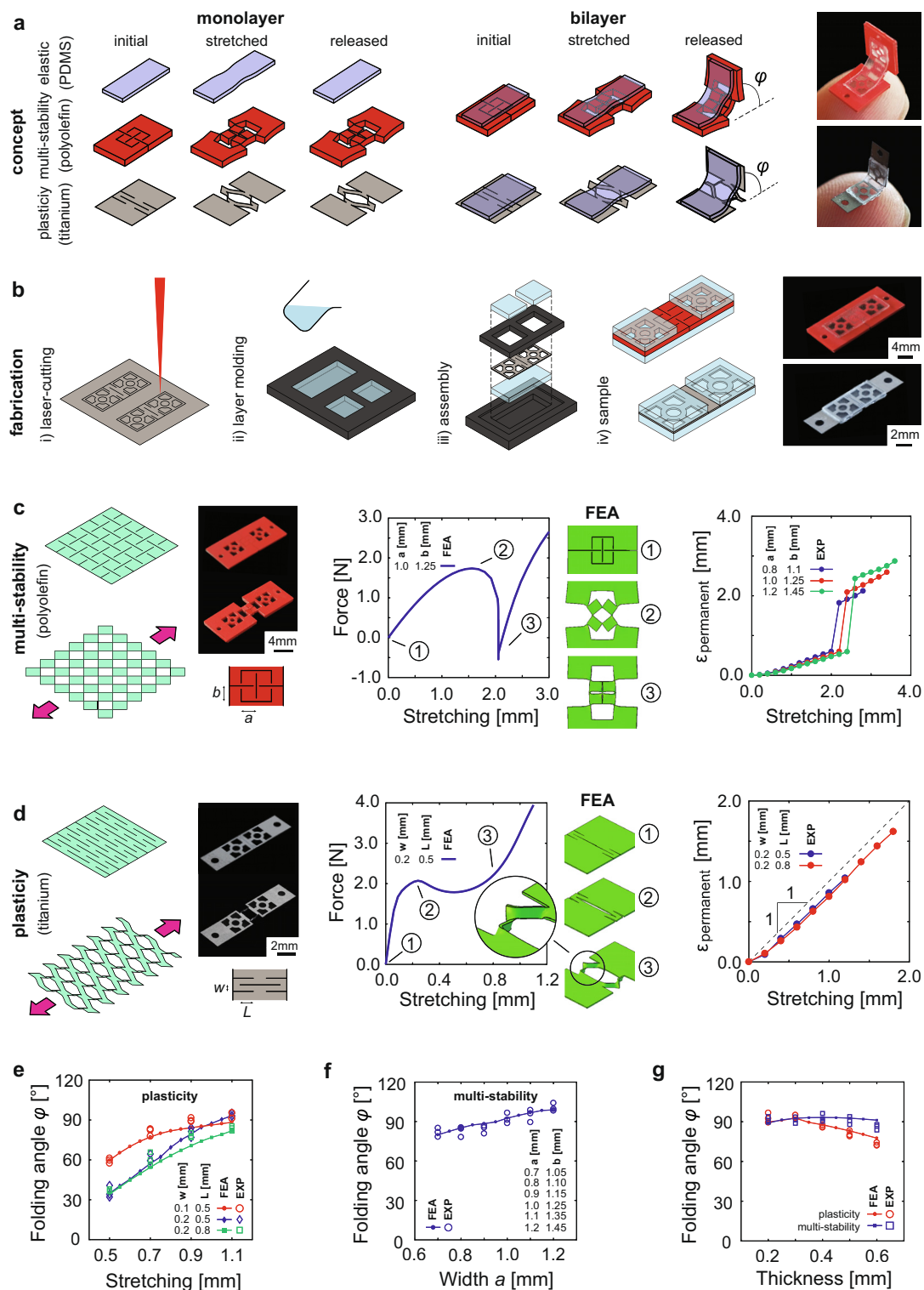
FIGURE 1

The main concepts and methods used for the design and fabrication of self-folding elements. (a) Two types of basic elements were designed by combining two types of permanently-deforming kirigami-based monolayers with an elastic layer to create bilayers (left). Stretching the bilayers resulted in self-folding elements that exhibited out-of-plane bending upon releasing the force (right). (b) The kirigami elements were made by laser cutting after which they were assembled with molded PDMS layers to create the basic elements. (c) One type of the kirigami elements were made from a polymeric material and worked through multi-stability (left). In this design, the four squares constituting the middle part of the kirigami element rotated as the force gradually increased until they snapped to another position at which point the force drops (middle). The amount of permanent deformation as a function of the design parameters and stretching was measured (right). (d) The other type of kirigami elements was made from a metallic foil (left) and worked on the basis of plastic deformation resulting from localized out-of-plane buckling (middle). Permanent deformation as a function of the design parameters and stretching was measured (right). (e–g) The folding angle as a function of design parameters and stretching (e), width (f), and thickness of the elastic layer (g) (both experimental and FEA values). See Supplementary video 1.

ligaments or the properties of the used materials might affect the permanent elongation as well, but were not considered here.

In the case of metal foils, high levels of plastic deformation were achieved by incorporating a pattern of parallel grooves into a titanium foil (Fig. 1d). Using this approach, the maximum amount of the allowable permanent deformation was increased by more than two orders of magnitude to values >100% strain (Fig. 1d). In these kirigami patterns, the deformation is localized at the edges of the cut patterns (Fig. 1d). The thinly cut ribbons stretch up to the point where localized deformation leads to a highly localized out-of-plane buckling at the sharp corners of the cut pattern (Fig. 1d). Given that this deformation is plastic in the case of metal foils, the kirigami strip is permanently elongated. Our experiments showed that the amount of permanent elongation equals the level of stretching, except for a small offset caused by the recovery of the initial elastic response of the material (Fig. 1d). Depending on the applied stretching, the thickness of the elastic layer, and the dimensions of the kirigami cutting patterns, folding angles up to 100° could be achieved (Fig. 1e–g). The folding angles generally increased with the applied stretching (Fig. 1e). The folding angles predicted by our finite element analysis (FEA) models were in excellent agreement with the experimentally observed values (Fig. 1e), meaning that these models could be used for the rational design of the self-folding elements (e.g., dimensions, cut-patterns, etc.). Regarding the bistable self-folding elements, a larger width of the rotating square elements resulted in higher folding angles (Fig. 1f). The thickness-dependency of the folding angle was much more severe in the case of plastically deforming kirigami elements, while there was little to no such dependency in the case of the multi-stable elements (Fig. 1g). Supplementary video 1 demonstrates how both types of basic elements work in practice.

Arrays of self-folding elements

To create more complex shape-shifting behaviors, one needs to use assemblies of these two basic elements. The advantage of the plastically deformed kirigami elements is that they allow for a continuous range of elongations, while multi-stable elements work on the on–off basis, meaning that only certain discrete values of elongation are admissible. Moreover, multi-stable elements require a minimum ratio of their thickness to the other dimensions to exhibit the specific snap-through instability behavior that is required for inducing permanent elongation [65]. Nevertheless, multi-stable elements have an important feature that makes them particularly useful for complex assemblies of basic elements, namely the elongation of the multi-stable elements assembled in-series is largely independent of each other. That does not hold for the plastically deforming kirigami elements, where four stages of deformation are observed in the simplest case of two in-series assembled elements (Fig. 2a and b). In the first stage (stage I, Fig. 2a and b), both elements elongate together until one of them experiences localized buckling after which elongation will occur mostly in that element (stage II, Fig. 2a and b). This continues up to the point where the second element also experiences localized buckling following which only the second element will elongate (stage III, Fig. 2a and b). Once both elements have equally elongated, they will again start to elongate together (stage IV, Fig. 2a and b). Our experimental measurements clearly showed the presence of these four stages and the difference between the assembled elements in terms of their individual elongations (Fig. 2a).

We assembled the basic building blocks described above in series and in parallel (Fig. 2c–f). In-series positioning of the self-folding elements allowed for the formation of linear patterns with the same (Fig. 2c) and different folding angles (Fig. 2d). A
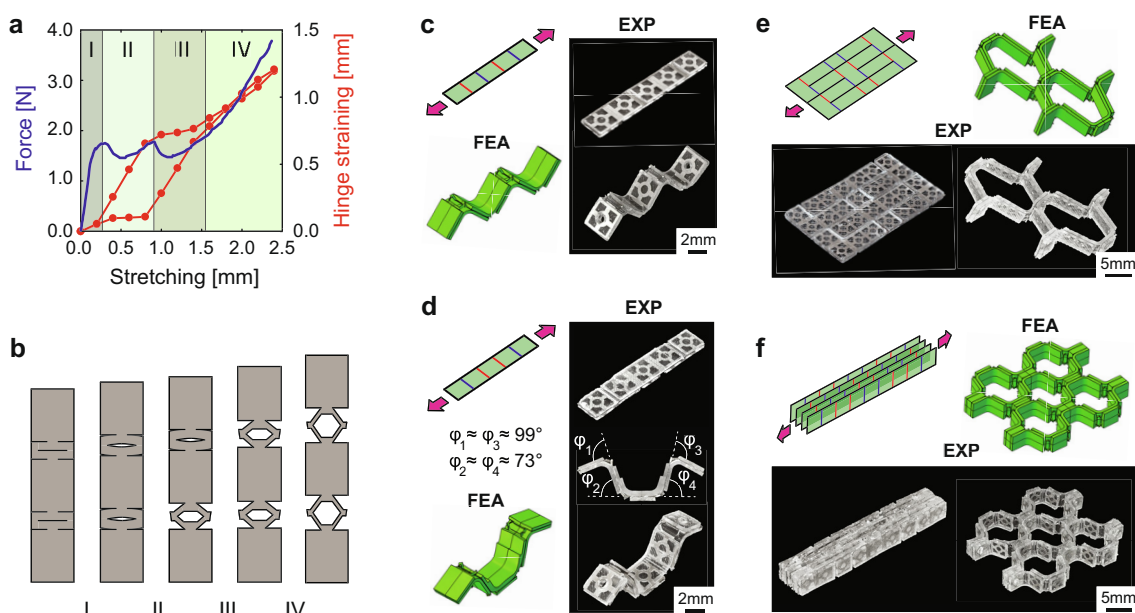
FIGURE 2

The self-folding behavior of the arrays of self-folding elements connected to each other in series and in parallel as predicted with FEA models and observed in our experiments. (a and b) Force and hinge straining as functions of stretching in the case of two basic elements connected to each other in series (a). Both basic elements do not deform simultaneously and four different stages of deformation can be identified (b). (c and d) Self-folding elements connected to each other in series with similar (c) and different (d) folding angles. (e and f) An array of self-folding elements connected in parallel and in-series to create more complex patterns of shape-shifting behavior. See Supplementary video 2.

combination of in-parallel and in-series assembly of the basic elements allowed for the fabrication of more complex 3D shapes with complex planar patterns (Fig. 2e and f). These patterns could be also stacked to create multi-storey constructs possibly with patterns that vary from one story to another. The level of stretching applied to the presented designs (Table 1) was determined using the results presented in Fig. 1e. Supplementary video 2 shows the self-folding behavior of the samples presented in Fig. 2.

Complex assemblies
The real challenge, however, is in the design of fully self-folding multi-storey structures. Indeed, the folding sequences devised for such multi-storey constructs as lattice origami require sequential folding. We combined orthogonal assemblies of the basic elements with stiff panels to enable the sequential self-folding of multi-storey constructs (Fig. 3). In this approach, stretching is performed sequentially: first along one of the orthogonal directions and, then, along the other. We fabricated three types of self-folding 3D designs including a cube and two multi-storey structures (Fig. 3). In all cases, we fabricated the specimens using both multi-stable and plastically deformed kirigami elements (Fig. 3). The deformed shapes of all structures were accurately predicted by our FEA models (Fig. 3), meaning that they could be used as a predictive tool for the rational design of complex assemblies of basic elements in general and for the design of the critical dimensions of both basic elements and orthogonal assemblies. We, therefore, chose the design parameters of the individual basic elements making up the assemblies such that they exhibited the differential self-folding response required for creating the multi-storey constructs. Given the dimensions of the plastically deforming assemblies ($w = 0.2$ mm, $L = 0.5$ mm, PDMS thickness = 0.3 mm) and a desired folding angle of 90°, these orthogonal assemblies were stretched by 1.05 mm (Fig. 1e) times the number of the folding units present in the assembly. The bistable self-folding elements ($a = 1.0$ mm, $b = 1.25$ mm, PDMS thickness = 0.3 mm) were strained by 2.5 mm times the number of the folding units present in the assembly to ensure that all the elements 'snapped' in their extended state. The applied levels of stretching for the designs presented in Fig. 3 are listed in Table 1. The activation sequences

and self-folding behavior of the specimens can be seen in Supplementary video 3.

Surface-related functionalities
To demonstrate some of the functionalities that could be incorporated into the self-folding origami-inspired structures developed here, we created specimens with two different types of surface-related functionalities including precisely-controlled surface micro-patterns and flexible electronics. Starting from a flat state enabled us to use optical lithography for incorporating a wide range of arbitrarily complex, precisely controlled, and spatially varied micropatterns (Fig. 4a) onto the PDMS layer during the curing process. In this way, the micro-patterns were incorporated in a single-step fabrication process. The flexible electronics were incorporated into our specimens using highly stretchable copper connectors that could accommodate the applied stretching during the self-folding process (Fig. 4b). Our coil-like designs of the connectors (Fig. 4b) was also effective in reducing the amount of strain that they underwent during the self-folding process. Our FEA models predicted that the dimensions of the connectors strongly affect the strains they experience during the self-folding process (Fig. 4b). For example, the maximum strain values predicted for the connectors increased by up to ≈ 3 folds when the width of the ribbon increased from 10 µm to 50 µm (Fig. 4b). This clearly shows the importance of high cutting precisions that allowed us to choose a width of 30 µm to simultaneously limit the maximum strain experienced by the connectors while avoiding the risk of failure in very thin connectors (e.g., connectors with a width of 10 µm). The amount of strain sustained by the connectors significantly decreased upon folding, and reached values ≤5% for folding angles between 45° and 90° (Fig. 4b). Since such a folding behavior is driven by the release of the pre-stress present in the PDMS layer, the strain of the copper circuit decreases as well. This decrease is, however, limited given the fact that copper has been plastically deformed. A micro-LED was incorporated in the design of a self-folding box to demonstrate the feasibility of integrating electronic devices into these origami-inspired self-folding structures (Fig. 4c). The micro-LED was then lit to confirm the proper connectivity of the circuits after self-folding (Fig. 4c, see Supplementary video 4).

TABLE 1

The parameters that were used for activation (*i.e.*, stretching) of the designs presented in this work.

Structure	Figure	Stretching [mm]
Series of identical basic elements	2c	4.2
Series of different basic elements	2d	4.0
Parallel strips of self-folding basic elements	2e	4.0
Stacked strips of self-folding basic elements	2f	8.0

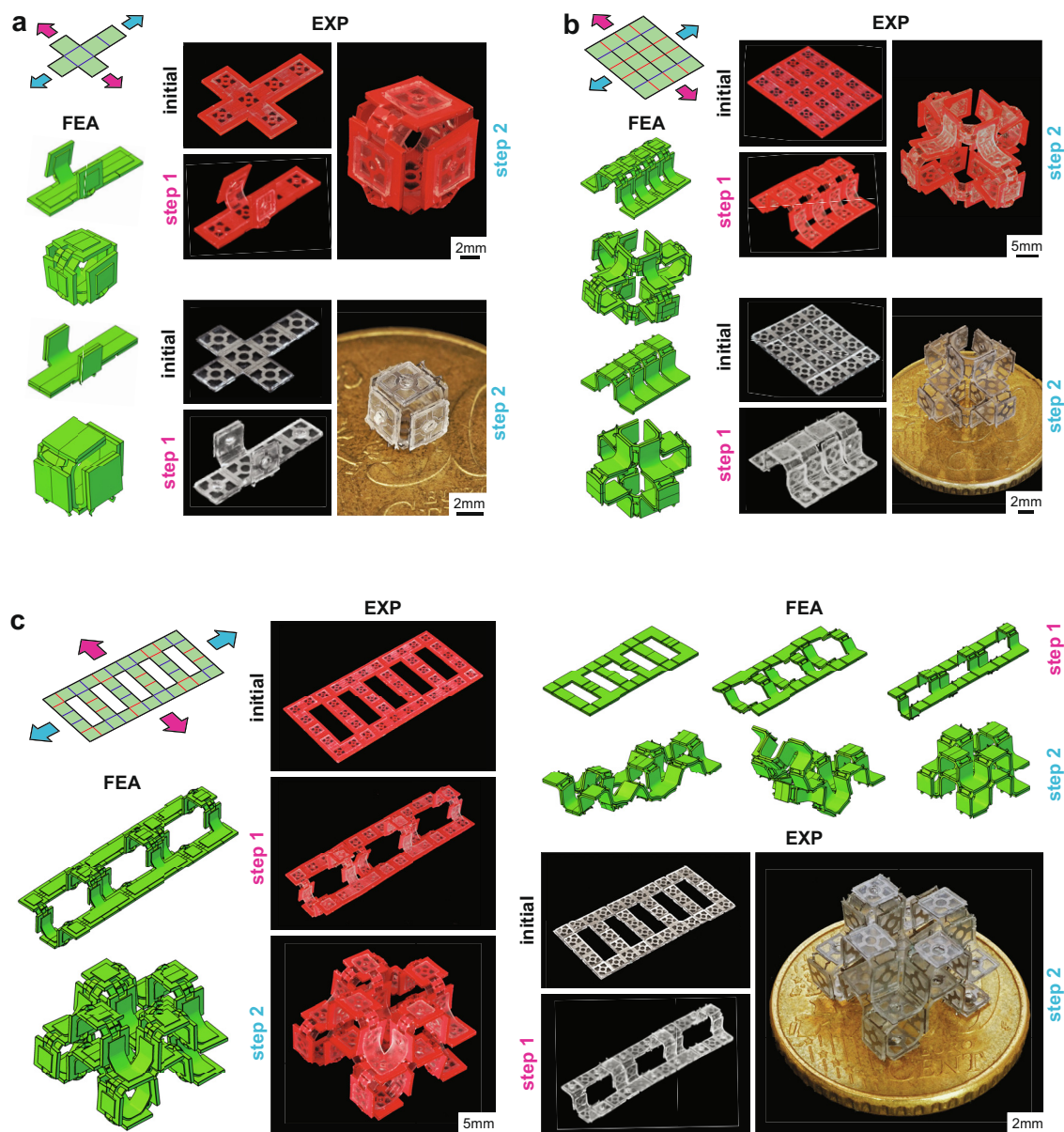| Structure	Figure	Stretching – step 1 [mm]	Stretching – step 2 [mm]
Cubic box – multi-stability	3a	5.0	7.5
Cubic box – plasticity	3a	2.1	3.15
Tubular construct – multi-stability	3b	10.0	7.5
Tubular construct – plasticity	3b	4.2	3.15
Multi-storey lattice – multi-stability	3c	10.0	25.0
Multi-storey lattice – plasticity	3c	4.2	10.5
Cubic box – micro LED	4c	2.1	3.15

FIGURE 3

Complex shape-shifting behavior for three different designs as predicted with FEA models and observed in our experiments. (a–c) Self-folding of a cube from a flat state (a) as well as sequential shape-shifting from flat states to complex multi-storey shapes (b and c). All designs were realized using both multi-stable (red) and plastically deforming (gray) kirigami elements. See Supplementary video 3.

One concern regarding the design of electric circuits is the effects of Joule heating on the shape-shifting behavior. By designing low resistance circuits embedded in a thermally stable matrix, such as PDMS, the rise in the temperature of the constructs upon application of current and the change in mechanical properties of the elastic layer can be minimized. Indeed, it may be possible to use amplified Joule heating in combination with heat-sensitive materials in alternative design approaches that aim to introduce some degrees of tunability into the self-folding specimens. Other aspects including the strains that the circuit is subjected to during actuation might affect the thermo-electric performance as well. Here, however, we focused on the irreversible fabrication of 3D geometries that, once completed, are not expected to change. This limits the consequences of any such effects to the fabrication stage.

Outlook and conclusions

In summary, we presented an approach for the fabrication of complex (e.g., multi-storey) self-folding origami-inspired structures that works on the basis of bilayers of permanently deforming kirigami elements and an elastic layer. Global mechanical forces activate the self-folding behavior. Given the highly mechanical nature of these elements, they could be made from a very wide range of materials at the micro-scale, which distinguishes this method from most other shape-shifting techniques that are either limited to specific materials or are limited to large-scale constructs (or both). We also demonstrated the possibility of incorporating bespoke micropatterns and flexible electronics into a number of 3D constructs made using this approach.
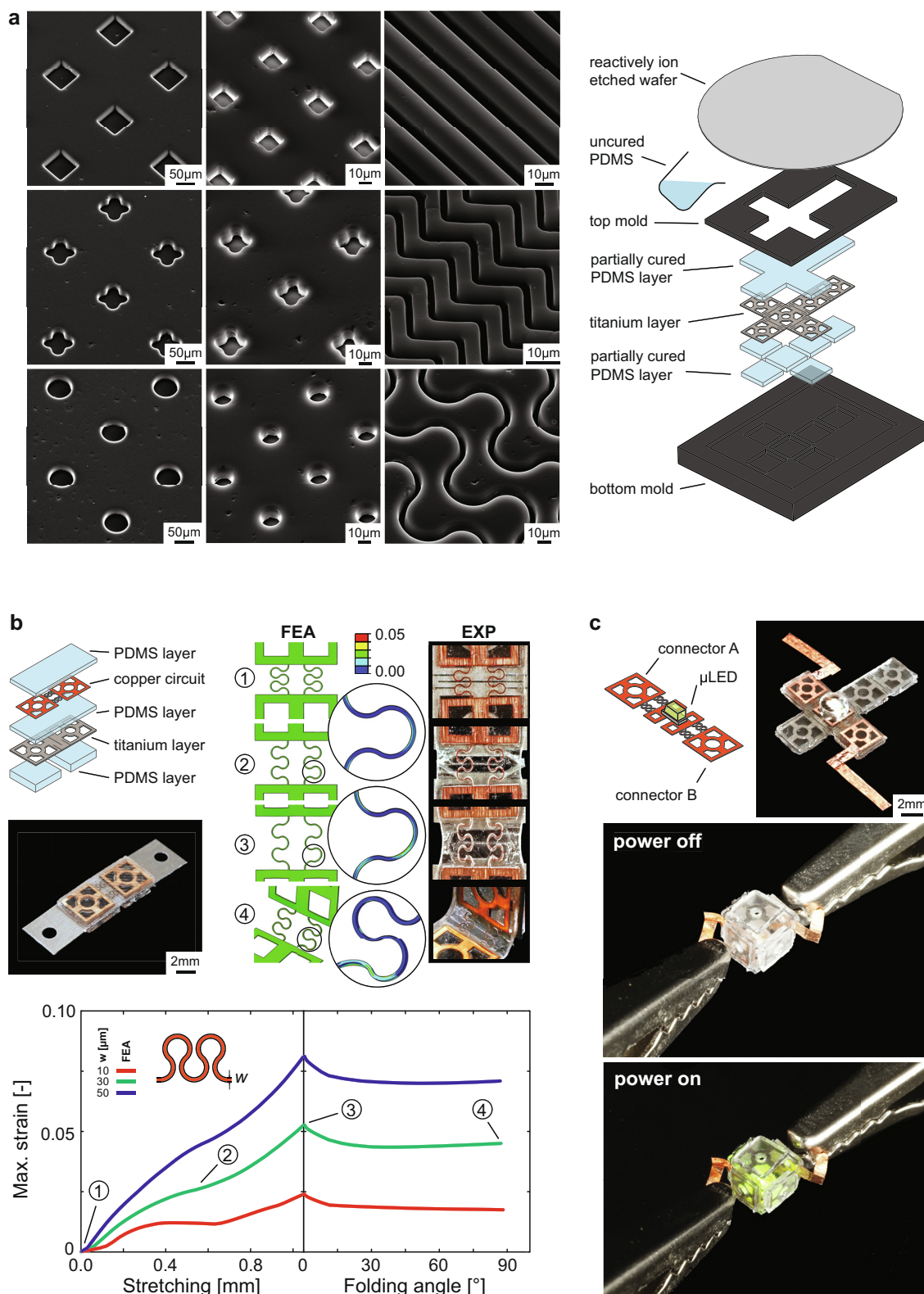
FIGURE 4

Surface-related functionalities added to our shape-shifting designs. (a) Precisely controlled, arbitrarily complex, and spatially varied micropatterns (left) created using optical lithography and molding in the elastic layer of our self-folding elements (right). (b) Flexible electronics incorporated into the design of the basic elements (top). FEA simulations were used to predict the strain in the flexible connectors and to study the effects of design parameters (*e.g.*, the width of the ribbons) on the experienced strain values (bottom). Experimentally observed and predicted shape-shifting behavior of the specimens incorporating flexible electronics agreed with each other (right). (c) A micro-LED was incorporated into a self-folding cube to demonstrate the feasibility of incorporating electronic devices in the presented designs. The micro-LED was lit to check the connectivity of the connectors after self-folding. See Supplementary video 4.

The two types of the basic kirigami elements used here harness either 'highly localized' mechanical instability or plastic deformations to create the desired patterns of self-folding. This allows us to create basic elements with easily predictable mechanical responses that could be assembled in a modular way to create more complex shape-shifting behavior without having to worry about the nonlinear post-buckling behavior of the geometrical designs resulting from such assemblies.

The feature sizes of the smallest specimens presented here (*e.g.*, Fig. 3) are in the micrometer range and are not far from the length-scales required for creating the 3D porous structures that could be used as tissue engineering scaffolds. This is the first time ever that such self-folding 3D porous structures are fabricated at this scale from biocompatible materials (*e.g.*, titanium foils) and with the possibility of directly incorporating micro-/nanopatterns that could influence stem cell differentiation [36–38] and kill bacteria to prevent implant-associated infections [39,40]. The demonstrated possibility to integrate flexible electronics could also pave the way for the development of smart implantable devices with sensing and on-demand drug delivery mechanisms. Such level of multi-functionality is unprecedented for implantable medical devices. This type of fabrication techniques could also be used in many other areas of advanced functional materials including micro-robotics, miniaturized steerable medical instruments, and precision devices. Finally, the mechanical nature of the proposed self-folding process also means that the functionality-inducing features or devices present on the surface are not affected by the chemicals or the high temperatures used in the activation process. This could be of importance for many of the application areas mentioned above.

Materials and methods

The multi-stable specimens were fabricated from polyolefin polymers (polyolefin, thickness = 0.65 mm; G. Apex, Taiwan Yun Lin Electronic Co. Taiwan) while plastically deforming kirigami were made from pure titanium foils (titanium foil, purity = 99.6+%, annealed, thickness = 50 μm; Goodfellow, UK). In both cases, the specimens were cut using laser micromachining (Optec Laser Micromachining Systems, Belgium). The permanently deforming kirigami constructs were then molded into a polydimethysoloxane (PDMS) elastomer matrix (Sylgard 184, Dow Corning, USA). The PDMS was thoroughly mixed (mixing ratio 7.5:1 between pre-polymer and curing agent) for at least 3 min followed by degassing for 10 min before being poured into the mold. The molds were made from acrylonitrile butadieen styrene (ABS) using 3D printers (Ultimaker 2+, Ultimaker, The Netherlands) that worked on the basis of fused deposition modeling (FDM). Both the polyolefin and titanium specimens were covered by a thin layer of a release agent (polyvinylalchohol (PVA), Polyestershoppen BV, The Netherlands) in order to minimize the adhesion between the kirigami specimens and the elastomeric layers. The individual layers of PDMS were (partially) cured for 60 min at 55 °C. In a second step, the individual layers together with the metal or polymer layer were assembled into another mold while some uncured PDMS was added to bond the partially cured PDMS layers together. As a final step, the specimens were fully cured for 24 h at 55 °C.

Various micro-scale patterns were produced on the surface of PDMS layers using replication of negatively designed micropatterns on a silicon wafer. The designed patterns were used to fabricate a photomask (optical photomask, feature size accuracy = 0.5 μm, Computographics Photomask Solutions, UK). A polished silicon wafer (4 inches, thickness = 525 ± 25 μm, p-type) was then cleaned with nitric acid (Merck, Darmstadt, Germany) followed by baking for 10 min in an oven at 110 °C for dehydration. Hexamethyldisilazane (HMDS) (BASF, Ludwigshafen, Germany) was poured on the surface at 150 °C for 45 s to improve the adhesion between the silicon substrate and photoresist. The process followed by spin coating a Shipley S1813 photoresist (MicroChem Corp., Newton, MA, USA) onto the wafer and baking at 115 °C on a hotplate for 60 s. Optical lithography was then carried out by an EVG 620 mask aligner (EVGroup, St. Florian, Austria), and the exposed resist was developed in MF-321 (Shipley, Microposit Developer, USA) at room temperature for 1.5 min, and rinsed in deionized water.

The patterns were transferred into the silicon wafer using an inductive coupled plasma reactive ion etching (ICP RIE) (Adixen, AMS100 Bosch, l-speeder) with SF6 = 200 sccm, C4F8 = 100 sccm, ICP power = 2000 W, CCP = 80 W, temperature = 10 °C, and for 5 min. The specimens were finally cleaned in acetone. To remove the HMDS layer, the samples were soaked in n-methylpyrrolidon (NMP, Merck, Darmstadt, Germany) at 70 °C for 5 min and then in resist stripper (PRS-3000, JTBaker, The Netherlands) for 10 min and at 80 °C. Finally, the specimens were rinsed thoroughly in DI water and then spin-dried. The final cleaning process was done by oxygen plasma (Tepla M4L Gas Plasma System, Corona, CA, USA) with O2 flow = 200 sccm, power = 600 W, and for 10 min.

Conductive circuits were made from a copper foil (copper foil, purity = 99.9+%, annealed, thickness = 25 μm; Goodfellow, UK) using laser micromachining. Electrical components were adhesively bonded to the circuit using conductive glue (wire glue, Anders Products, MA, USA). A layer of ethyl cyanoacrylate (LOCTITE 401, Loctite, Germany) adhesive was added to increase the bonding strength between the circuit and the electronic devices.

The self-folding specimens were stretched using a Lloyd LR5K mechanical testing machine equipped with either a 5 N or 100 N load cell (depending on the range of the measured forces). The deformations experienced by the specimens were captured using a high-resolution digital camera (Sony A7R with a Sony FE 90-mm f/2.8 macro OSS lens). Image processing was used for measuring the folding angle of the basic elements.

FEA was performed using the commercial software Abaqus (Abaqus 6.14). An implicit nonlinear solver (Abaqus Standard, full Newton method) was used to simulate both the stretching and folding of the plastically deforming self-folding constructs. First, a linear buckling analysis was performed to find the buckling modes of the specimens. The first buckling mode predicted by the linear buckling analysis was then introduced as an imperfection to predict the post-buckling behavior of the specimens. Full-integrated solid elements (*i.e.*, C3D8 or C3D20) were used to model the titanium specimens. The PDMS layers were modeled using eight-node hybrid solid elements (*i.e.*, C3D8H). A surface-to-surface contact definition between the titanium and PDMS layers was implemented using a penalty contact

enforcement algorithm. For the complex assemblies, the contact definition was replaced by a number of constraint equations, thereby enhancing the convergence while limiting the required computational cost.

A dynamic analysis using the same nonlinear implicit solver was performed to model the multi-stable behavior of the self-folding hinges. Eight-node hybrid solid elements (*i.e.*, C3D8H) were used for modeling both polyolefin and PDMS layers. A self-contact definition was implemented in order to prevent self-penetration of the polyolefin surfaces. Similar to the case of titanium specimens, a penalty contact enforcement algorithm was used.

The stretching and folding of the self-folding hinges embedded with an electrical circuit were also analyzed using FEA (Abaqus Standard). The copper circuit was modeled using eight-node solid elements (*i.e.*, C3D8) and an elastoplastic material model (von Mises yield function, tabular input of strain hardening data) based on a stress–strain curve reported in the literature [66]. Constraint equations between the adjacent nodes of the PDMS and the copper layers were applied to ensure the embedding of the copper circuit inside the PDMS matrix.

Uniaxial tensile tests were performed to characterize the mechanical properties of titanium, polyolefin, and PDMS using the same mechanical testing machine (100 N load cell). An elastoplastic material model (von Mises yield function, tabular input of strain hardening data) was fitted to model the mechanical behavior of titanium. Incompressible hyperelastic material models were used for the modeling of both polyolefin (3rd order Ogden model) and PDMS (2nd order Ogden model). More details can be found in the Supplementary material.

Data availability

All data used to generate these results is available in the main text or Supplementary material.

Acknowledgment

Appendix A. Supplementary data

Supplementary data to this article can be found online at https://doi.org/10.1016/j.mattod.2019.08.001.

References

[1] Y. Liu, J. Genzer, M.D. Dickey, Prog. Polym. Sci. 52 (2016) 79–106.
[2] C.D. Santangelo, Annu. Rev. Condens. Matter Phys. 8 (2017) 165–183.
[3] T. van Manen, S. Janbaz, A.A. Zadpoor, Mater. Today 21 (2018) 144–163.
[4] M. Boyvat, J.-S. Koh, R.J. Wood, Robotics 2 (2017) eaan1544.
[5] S. Felton et al., Science 345 (2014) 644–646.
[6] J. Mu et al., Sci. Adv. 1 (2015) e1500533.
[7] Z.E. Teoh et al., Robotics 3 (2018) eaat5276.
[8] V.B. Shenoy, D.H. Gracias, MRS Bull. 37 (2012) 847–854.
[9] K. Bertoldi et al., Nat. Rev. Mater. 2 (2017) 17066.
[10] J.T. Overvelde et al., Nat. Commun. 7 (2016) 10929.
[11] J.L. Silverberg et al., Science 345 (2014) 647–650.
[12] Z. Wang et al., Adv. Mater. 29 (2017) 1700412.
[13] H. Yasuda, J. Yang, Phys. Rev. Lett. 114 (2015) 185502.
[14] J.H. Cho et al., Small 7 (2011) 1943–1948.
[15] S. Sundaram et al., ACS Appl. Mater. Interfaces 9 (2017) 32290–32298.
[16] G.J. Hayes et al., IEEE Trans. Antennas Propag. 62 (2014) 5416–5419.
[17] D. Hartl, K. Lane, R. Malak (Eds.), ASME 2012 Conference on Smart Materials, Adaptive Structures and Intelligent Systems, American Society of Mechanical Engineers, 2012, pp. 277–285.
[18] D. Hartl, K. Lane, R. Malak (Eds.), ASME 2012 International Mechanical Engineering Congress and Exposition, American Society of Mechanical Engineers, 2012, pp. 115–122.
[19] S. Janbaz, R. Hedayati, A. Zadpoor, Mater. Horiz. 3 (2016) 536–547.
[20] S. Janbaz et al., Sci. Adv. 3 (2017) eaao1595.
[21] K. Kuribayashi-Shigetomi, H. Onoe, S. Takeuchi, PLoS ONE 7 (2012) e51085.
[22] Y. Chen et al., Phys. Rev. Appl. 7 (2017) 024012.
[23] R. Hedayati, A. Leeflang, A. Zadpoor, Appl. Phys. Lett. 110 (2017) 091905.
[24] M. Kadic et al., Appl. Phys. Lett. 100 (2012) 191901.
[25] J.-H. Lee et al., Nano Lett. 12 (2012) 4392–4396.
[26] Q. Wang et al., Phys. Rev. Lett. 117 (2016) 175901.
[27] X. Zheng et al., Science 344 (2014) 1373–1377.
[28] D.H. Kim et al., Adv. Mater. 22 (2010) 4551–4566.
[29] S.O. Kim et al., Nature 424 (2003) 411.
[30] S. Yang et al., Adv. Funct. Mater. 21 (2011) 2446–2455.
[31] Y. Narui, K.S. Salaita, Chem. Sci. 3 (2012) 794–799.
[32] C.C. Wu et al., Small 7 (2011) 989–1002.
[33] A. Mackus et al., Nanoscale 4 (2012) 4477–4480.
[34] J. Du (Ed.), Proceedings of the Twelfth International Conference on Tangible, Embedded, and Embodied Interaction, ACM, 2018, pp. 166–176.
[35] S. Rus (Ed.), European Conference on Ambient Intelligence, Springer, 2018, pp. 147–161.
[36] W. Chen et al., Nano Today 9 (2014) 759–784.
[37] M.J. Dalby, N. Gadegaard, R.O. Oreffo, Nat. Mater. 13 (2014) 558.
[38] S. Dobbenga, L.E. Fratila-Apachitei, A.A. Zadpoor, Acta Biomater. 46 (2016) 3–14.
[39] D.P. Linklater, S. Juodkazis, E.P. Ivanova, Nanoscale 9 (2017) 16564–16585.
[40] K. Modaresifar et al., Acta Biomater. (2018).
[41] B. Bhushan, Y.C. Jung, J. Phys.: Condens. Matter. 20 (2008) 225010.
[42] B. Bhushan, Y.C. Jung, K. Koch, Philos. Trans. Royal Soc. A 367 (2009) 1631–1672.
[43] E. Martines et al., Nano Lett. 5 (2005) 2097–2103.
[44] S.J.P. Callens, A.A. Zadpoor, Mater. Today 21 (2018) 241–264.
[45] M. Behl, A. Lendlein, Mater. Today 10 (2007) 20–28.
[46] X. Shen et al., Nat. Chem. 5 (2013) 1035.
[47] J. Cui, F.R. Poblete, Y. Zhu, Adv. Funct. Mater. 28 (2018) 1802768.
[48] M. Ma et al., Science 339 (2013) 186–189.
[49] A.S. Gladman et al., Nat. Mater. (2016).
[50] T. van Manen, S. Janbaz, A.A. Zadpoor, Mater. Horiz. (2017).
[51] Y. Zhang et al., Nat. Rev. Mater. 2 (2017) 17019.
[52] D.H. Gracias et al., Adv. Mater. 14 (2002) 235–238.
[53] S. Pandey et al., Proc. Natl. Acad. Sci. 108 (2011) 19885–19890.
[54] S. Xu et al., Science 347 (2015) 154–159.
[55] M. Jamal, A.M. Zarafshar, D.H. Gracias, Nat. Commun. 2 (2011) 527.
[56] Y. Liu et al., Soft Matter 8 (2012) 1764–1769.
[57] H. Fu et al., Nat. Mater. 17 (2018) 268.
[58] S. Waitukaitis et al., Phys. Rev. Lett. 114 (2015) 055503.
[59] Y. Yang, M.A. Dias, D.P. Holmes, Phys. Rev. Mater. 2 (2018) 110601.
[60] R.M. Neville et al., Smart Mater. Struct. 26 (2017) 05LT03.
[61] R.M. Neville, F. Scarpa, A. Pirrera, Sci. Rep. 6 (2016) 31067.
[62] K. Saito, F. Agnese, F. Scarpa, J. Intell. Mater. Syst. Struct. 22 (2011) 935–944.
[63] T.C. Shyu et al., Nat. Mater. 14 (2015) 785.
[64] R. Sun et al., Appl. Phys. Lett. 112 (2018) 251904.
[65] A. Rafsanjani, K. Bertoldi, Phys. Rev. Lett. 118 (2017) 084301.
[66] G. Simons et al., Mater. Sci. Eng., A 416 (2006) 290–299.